Journal of Materials Science: Materials in Electronics (2018) 29:16765–16774
https://doi.org/10.1007/s10854-018-9770-0

Hydrothermal synthesis of nanomoss Nb_2O_5 films and their ultraviolet photodetection performance

Rozina Abdul Rani[1,2] · Ahmad Sabirin Zoolfakar[2] · Nur Samihah Khairir[2] · Mohamad Hafiz Mamat[2] · Salman Alrokayan[3] · Haseeb A. Khan[3] · Mohamad Rusop Mahmood[1,2]

Received: 1 February 2018 / Accepted: 27 July 2018 / Published online: 1 August 2018

Abstract
Hydrothermal process is one of the most suitable and highly controlled synthesis methods for engineering or tailoring the nanostructures of metal oxide. In the present work, etching agent assisted hydrothermal process was employed to synthesis nanostructured Nb_2O_5. Nanomoss Nb_2O_5 films were successfully synthesized on niobium foil in the ammonia fluoride based solution with concentration of 0.5 and 1.65 M at 95 °C for 24 h. Material analysis of the nanomoss Nb_2O_5 was carried out by field emission scanning electron microscopy, atomic force microscopy, X-ray diffraction (XRD), Fourier Transform Infrared Spectroscopy analysis and Ultraviolet–visible spectroscopy. The XRD characterization revealed that the nanomoss Nb_2O_5 only become crystalline after annealing for 60 min at 440 °C. That annealing condition also contributes to the growth of hump structure on the nanomoss films. Furthermore, it was observed that the films produce low reflectance properties in the range of 2.73–26.0% at UV wavelengths, which make them a potential candidate in UV sensor applications. To fabricate the UV sensor, platinum (Pt) electrode was deposited as a contact pad. Based on the UV characterization, the UV sensor based on nanomoss Nb_2O_5 films exhibited good photosensitivity of 2.0 and response time in the range of 51.4–76.8 s when exposed under turn on/off of UV light (365 nm, 750 μW/cm^2) at a bias voltage of 10 V.

1 Introduction

A lot of effort has been taken to synthesis a novel structure of metal oxide in order to enhance the properties of metal oxide for a better device performance. Several techniques to synthesis Niobium oxide (Nb_2O_5) has been reported such as hydrothermal [1–3], anodization [4–7], electrodeposition [8, 9], sol–gel spin-coating [10–12], sputtering [13–16] and pulse laser deposition [17, 18]. Due to their desirable properties such as stability in air and water, resistance to acid and base, low film stress, wide band gap and high refractive index, Nb_2O_5 can be one of the potential functional material for a lot of applications [15, 19, 20].

Generally, hydrothermal technique offer many advantages over other synthesis methods due to their facile process steps, low cost and environmental friendly process. This technique has been successfully applied to synthesis many types of Zinc oxide (ZnO) and Titanium oxide (TiO_2) nanostructures [21–27]. However, the hydrothermal based nanostructured Nb_2O_5 is not extensively investigated and their structure variations are also limited. Nb_2O_5 synthesis via hydrothermal technique normally involved interaction between ionic source of niobium metal (in powder form) in an acid or base, or the dissolution of a niobium salt such as niobium chloride, niobium ethoxide, or ammonium niobium oxalate in a solution which is heated at an elevated temperature for a certain period of time [19]. Lately, direct hydrothermally formed nanorods, nanotrees and nanowires of Nb_2O_5 on niobium (Nb) foil substrate have been synthesized at a temperature more than 100 °C in an autoclave containing etching agent based solution [1, 2, 28–30]. The possibility of controlled fabrication on direct substrate has

✉ Rozina Abdul Rani
rozina.abdulrani@yahoo.com

✉ Mohamad Rusop Mahmood
nanouitm@gmail.com

[1] NANO-SciTech Centre, Institute of Science, Universiti Teknologi MARA, 40450 Shah Alam, Selangor, Malaysia

[2] NANO-ElecTronic Centre, Faculty of Electrical Engineering, Universiti Teknologi MARA, 40450 Shah Alam, Selangor, Malaysia

[3] Research Chair for Biomedical Applications of Nanomaterials, Biochemistry Department, College of Science, King Saud University, Riyadh 11451, Saudi Arabia

significantly promotes fast device fabrication and provides more opportunity to utilize the unique properties of present nanomaterials.

At the moment, the etching assisted hydrothermal based Nb_2O_5 films on Nb foil substrate has been studied for the UV sensor (Nb_2O_5 nanobelts) [29], energy storage (Nb_2O_5 nanorods) [2] and gas sensor (Nb_2O_5 nanorods) [31] applications. Fang et. al. have examined single Nb_2O_5 nanobelts as a sensing material for visible-blind UV light sensors (the UV-A band between 320 and 400 nm). They found that the single Nb_2O_5 nanobelts exhibited great photoresponsivity of 15.2 A/W and long term stability of the photocurrent over a period of 2500 s at an applied voltage of 1.0 V [29]. Thus, it is believe that Nb_2O_5 is a promising candidate for high performance UV sensors and interesting to explore Nb_2O_5 as UV sensors with different nanostructures. In this study, we report the synthesis of nanomoss Nb_2O_5 films on Nb foil via a hydrothermal technique assisted with NH_4F as an etching agent at a temperature lower than 100 °C. The hydrothermal technique is conducted using Reagent glass bottle instead of autoclave in the hot water bath which is promoting for low cost and simple process. We study the nanomoss Nb_2O_5 films properties including surface morphology, structure, chemical bonding and optical reflection properties. The performance of fabricated UV sensor based nanomoss Nb_2O_5 films is also presented.

2 Materials and methods

2.1 Synthesis of niobium oxide

Niobium (Nb) foil with thickness of 0.25 mm was used as initial material in this experiment. The foils were cleaned with acetone, washed with deionized water and then dried at room temperature (RT). The Nb_2O_5 films were prepared via an etching agent—assisted hydrothermal synthesis process. In this experiment, ammonium fluoride (NH_4F) was used as an etching agent. Solution with concentration of 0.5 and 1.65 M of NH_4F in deionized water (DIW) was prepared. After stirring the solution for 30 min, the Nb foils with dimension of 1.0 cm × 1.5 cm was put into NH_4F aqueous solution and kept at 95 °C in water bath for 24 h. Then, the samples were washed with deionized water and dried at RT. The samples underwent the annealing process in air at temperature of 440 °C for 40 and 60 min. The selection of 440 °C as an annealing temperature is based on the previous work [32]. Summary of the synthesis parameter of Nb_2O_5 films was presented in Table 1.

Table 1 Synthesis parameter of nanomoss Nb_2O_5 films

Sample	NH_4F concentration (M)	Annealing condition (temperature/time)
A	0.5	440 °C/40 min
B	0.5	440 °C/60 min
C	1.65	440 °C/40 min
D	1.65	440 °C/60 min

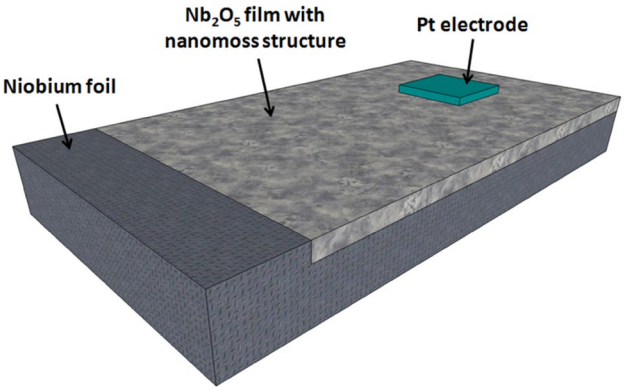

Fig. 1 Schematic diagram of nanomoss Nb_2O_5 films based UV sensor

2.2 UV sensor fabrication

For device fabrication, Platinum (Pt) electrode with the thickness of ~ 30 nm was deposited on top of the Nb_2O_5 films using a thermal evaporator at a deposition pressure of 4×10^{-4} Pa. The size of the Pt electrodes was 4 × 4 mm. The 3-dimensional configuration of the complete device is shown in Fig. 1.

2.3 Structural and device characterization

The obtained Nb_2O_5 morphological structures were characterized using a JEOL JSM-6700F field-emission scanning electron microscope (FESEM) and the crystallinity of the samples was characterised by X-ray diffraction (XRD, Panalytical X'pert PRO). The reflectance analysis of the samples was carried out using Ultraviolet–Visible (UV–Vis) Spectrophotometer Cary 5000, Varian. The Fourier transform infrared spectroscopy FTIR analysis was conducted using Spectrum 400 Perkin Elmer. The UV characterization measurements of the fabricated sensor were conducted using a UV photocurrent measurement system (Keithley 2400) operating at 365 nm with a power density of 750 μW/cm^2 at a bias voltage of 10 V.

3 Results and discussion

The FESEM image in Fig. 2 illustrate the morphological structure of the Nb_2O_5 films synthesized in two different concentrations of NH_4F based hydrothermal solution (0.5 and 1.65 M) and annealing duration (40 and 60 min). The images reveal that the Nb_2O_5 films contain nanomoss-like structure on their films surface. Nb_2O_5 films annealed for 40 min at temperature of 440 °C (sample A and C) which is presented in Fig. 2a, b show a uniform distribution of nanomoss structure. Meanwhile, increasing the annealing duration to 60 min has contributed to the formation of hump structures on the Nb_2O_5 films. For sample B of nanomoss Nb_2O_5 film which is presented in Fig. 2c, it is found that the diameter of hump is in the range of 500 nm to 1 µm. While for sample D (Fig. 2d), the diameter of hump are approximately between 2 and 4 µm when prepared in the concentration of 1.65 M NH_4F.

Figure 3 shows the three-dimensional (3D) AFM images of nanomoss Nb_2O_5 films synthesized using concentration of 0.5 and 1.65 M NH_4F and annealed at 440 °C for 40 and 60 min, respectively. Samples A and C which is annealed for 40 min have root mean square (RMS) surface roughness of ~ 37.30 and ~ 70.82 nm, respectively. Further increasing the annealing duration to 60 min has increased the surface roughness of the nanomoss Nb_2O_5 films due to the formation of hump structures on the films. The AFM results exhibited RMS surface roughness of 275 and 238 nm for sample B and D when annealed for 60 min, respectively. The reason

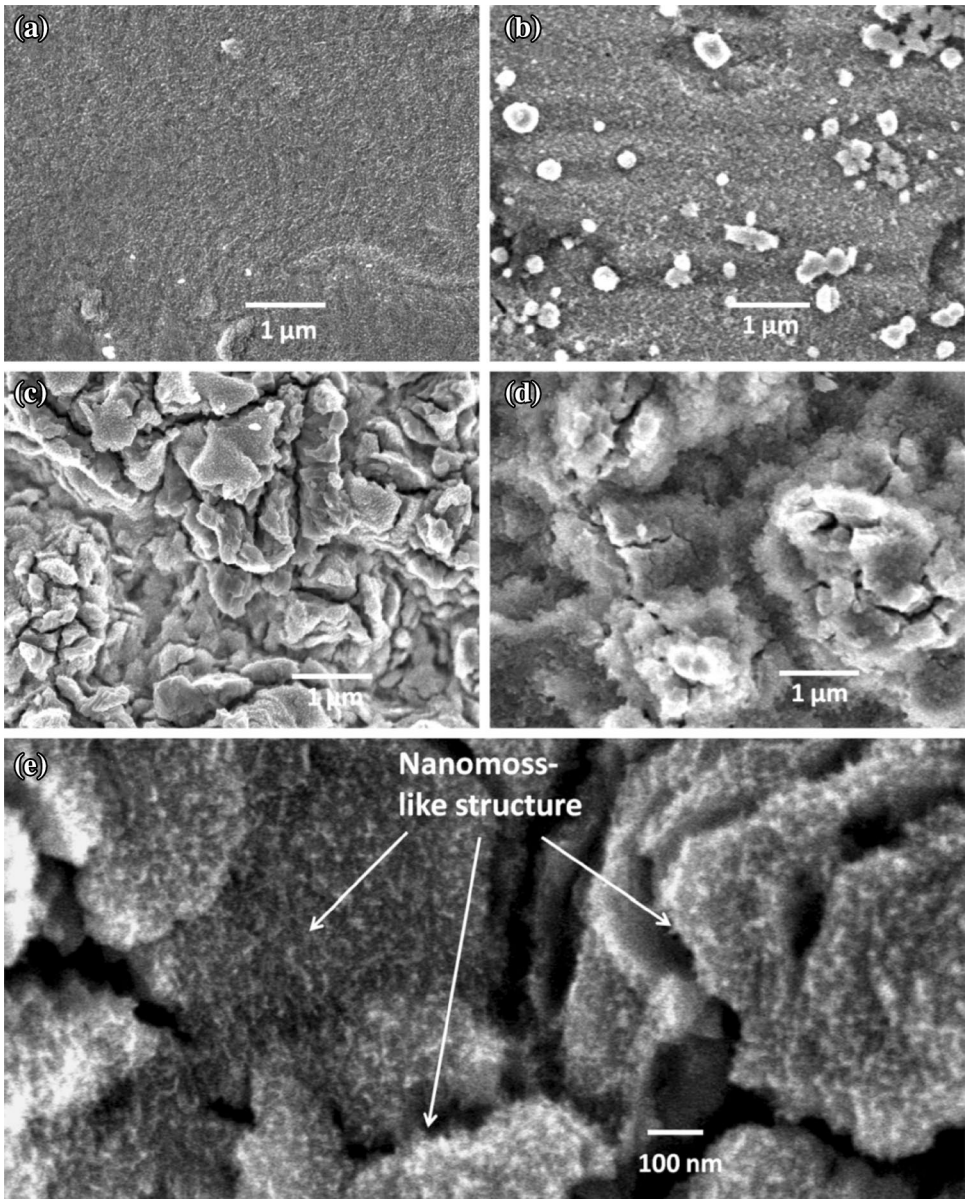

Fig. 2 FESEM images of nanomoss Nb_2O_5; **a** sample A, **b** sample C, **c** sample B and **d** sample D after the synthesis process in the NH_4F based hydrothermal solution at 95 °C for 24 h. The Nb_2O_5 films were annealed at 440 °C for **a**, **b** 40 min and **c**, **d** 60 min. **e** Higher magnification FESEM image (×60,000; 5.0 kV) shows the nanomoss-like structure on the surface of Nb_2O_5 film

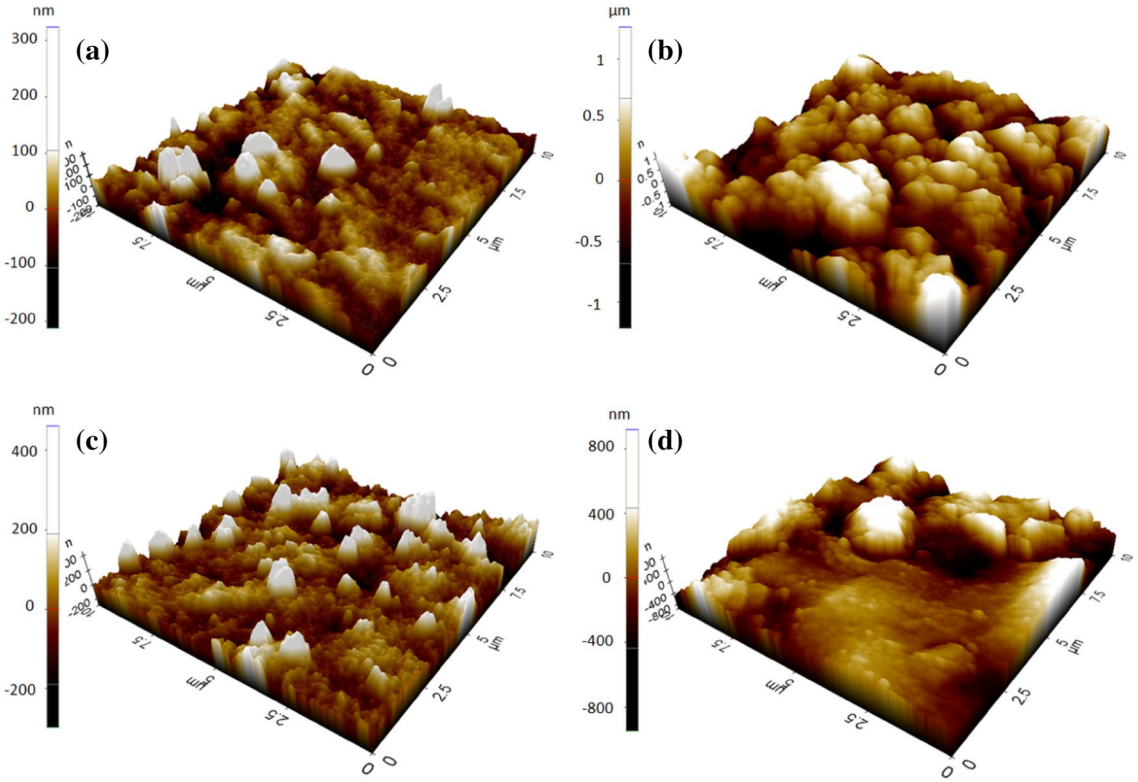

Fig. 3 3D Atomic Force Microscopy (AFM) images of 10×10 μm^2 size of nanomoss Nb_2O_5 films; **a** sample A, **b** sample B, **c** sample C and **d** sample D synthesized from NH_4F based hydrothermal solution at 95 °C for 24 h and annealed at temperature of 440°C

for sample B has higher RMS surface roughness value compared to sample D can be ascribed to the smaller hump size on the surface layer of sample B. These observations are consistent with the FESEM results presented in Fig. 2.

The formation of hump structure has contributed rough surface to Nb_2O_5 film, which is significantly affect the reflectance properties of the film. In material characterization, it is found that smaller grain size will increase scattering activity caused the absorptions to weaken and produced slightly higher reflectance spectra compared than larger grain size [33]. Thus, hump size of Nb_2O_5 films plays an important role. It is expected that the Nb_2O_5 films with larger hump size would produce low reflectance spectra and better performance of UV sensor.

For XRD analysis, only sample C and D are used. The XRD results of the nanomoss Nb_2O_5 films are shown in Fig. 4. From the XRD spectra, sample C has no other diffractions can be observed except for the Nb metal peaks at ~38.3, 55.2 and 69.2°, indicating that the film is not crystallized (appeared to be an amorphous). New diffraction peaks appear in the XRD pattern of the sample D when annealing duration was increased to 60 min. It is indicates that additional peaks exhibited at 22.8, 28.3, 42.6 and 49.9°. When increased the XRD 2θ scan range more than 50°, peak at 55.1, 58.4 and 69.1° are also observed. These peaks could

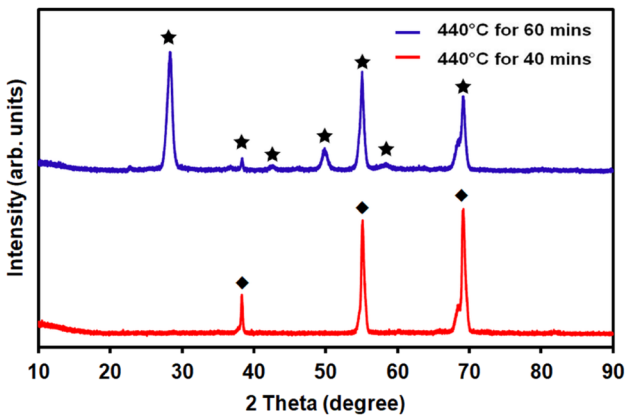

Fig. 4 XRD patterns of the Nb_2O_5 films synthesized in 1.65M NH_4F solution at 95 °C for 24 h and annealed for 40 min (sample C—red line) and 60 min (sample D—blue line) at temperature of 440 °C. Orthorhombic Nb_2O_5 is annotated by star while Nb metal is annotated by diamond. (Color figure online)

be indexed to the orthorhombic structure Nb_2O_5 (JCPDS No. 27-1003). Similar XRD pattern also reported in other works [32, 34, 35]. From the XRD spectra one can determine the full-width-at-half-maximum (FWHM) of a peak intensity profile, which can be used in the Scherrer formula to

estimate the average crystallite size [36]. The FWHM of the sample D estimated from the 28.3° peak is about 0.82 nm.

The properties of Nanomoss Nb_2O_5 films were further characterized by conducted FTIR spectroscopy. FTIR analysis normally used to reveal the bonding characteristics of functional groups in the prepared samples. In the FTIR spectra as presented in Fig. 5, the absorption peaks appear around wavenumber of 3400–1620 cm^{-1} can be associated to the asymmetric and symmetric stretching vibrations of the hydroxyls (–OH) group of absorbed water molecules and the surface hydroxyls. The peak appeared near 524 cm^{-1} (Sample A), 532 cm^{-1} (Sample B), 511 cm^{-1} (sample C) and 522 cm^{-1} (Sample D) corresponding to bridging Nb–O–Nb [37, 38]. Furthermore, peaks around 756 and 865 cm^{-1} in Sample A, corresponding to asymmetric stretching of [−O−Nb−O]n bonds [39]. Based on the appearance of all these peaks, it confirms the presence of Nb_2O_5. Then, peaks around 1065, 1170 and 1252 cm^{-1} also exhibited in the FTIR spectra due to stretching vibration of the C–O in Nb–O–C structure [40]. All the wavenumbers corresponding to each one of the absorptions is displayed in Table 2.

Table 2 IR absorptions observed in the FTIR spectra of the investigated nanomoss Nb_2O_5 films

Sample	A	B	C	D
Wavenumber (cm^{-1})	420	420	417	448
	448	453	450	489
	524	488	511	522
	695	532		
	756			
	801			
	841			
	865			
	1065			
	1170			
	1252			
	2966			

The reflectance of the nanomoss Nb_2O_5 films has been presented in Fig. 6. From the reflectance spectra, the reflectance range of 2.73–26.0% under ultra-violet wavelength (200–400 nm) has been produced by the films. Sample C and D synthesized in solution of 1.65M of NH_4F in DIW exhibited a very minimum reflectance around ~2.73 to 12.0% at a wavelength of 224–350 nm, respectively. Meanwhile, for sample A and B synthesized in solution of 0.5M of NH_4F in DIW, annealing at 60 min has significantly improved the reflectance properties of the films. It was observed that an improvement up to ~50% reduce of reflectance value can be archived when annealed the film at 60 min. This is in agreement with the study reported by Firoz Khan et al. that an improvement in the crystallinity of oxide films can significantly improved their reflectance properties (produced low reflection value) [41]. The obtained reflectance results have shown that this kind of Nb_2O_5 films is very suitable for anti-reflective coating layer and UV sensor application. Study on reflectance properties of Nb_2O_5 films is also reported by Coskun et al. where the minimum reflectance value of sputtered Nb_2O_5 films is about 8.12% at a wavelength of 375 nm [14]. Meanwhile, Dash et al. has produced sputtered Nb_2O_5 films with a reflectance value of ~10 to 20% in the visible

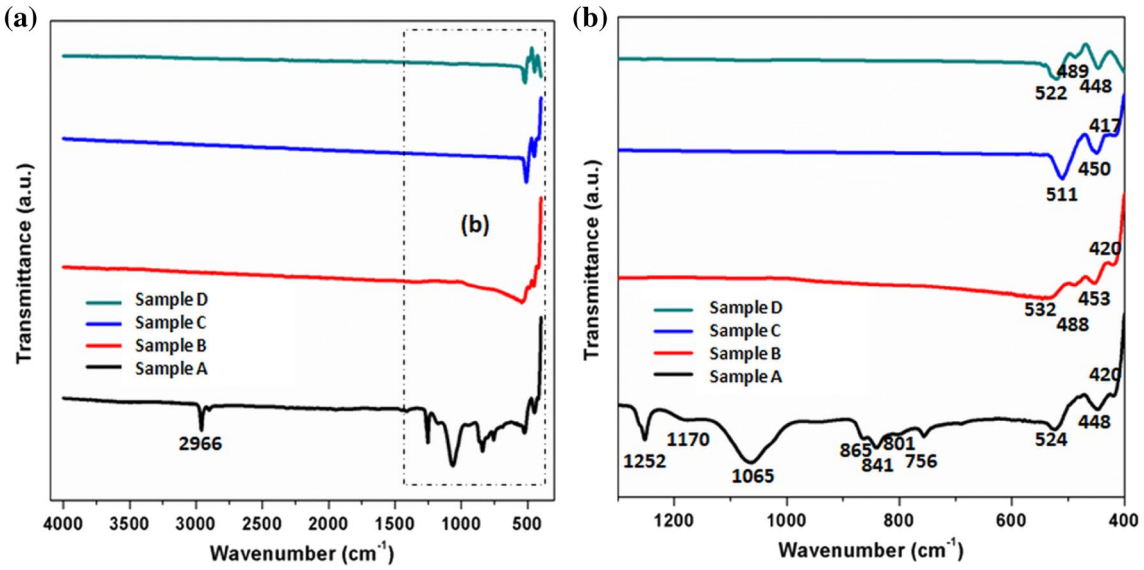

Fig. 5 FTIR spectra of nanomoss Nb_2O_5 films; sample A, sample B, sample C and sample D synthesized from NH_4F based hydrothermal solution at 95 °C for 24 h and annealed at temperature of 440°C

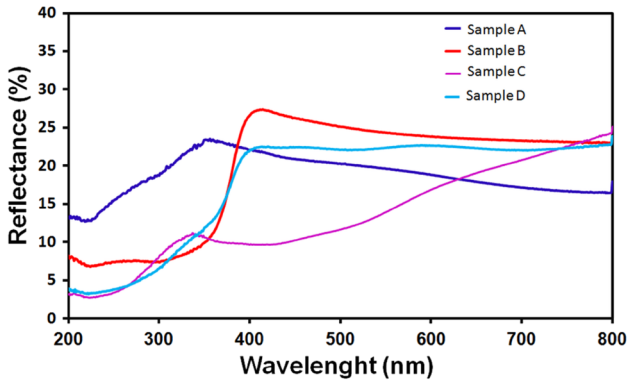

Fig. 6 Reflectance spectra of nanomoss Nb_2O_5 films; sample A, sample B, sample C and sample D synthesized from NH_4F based hydrothermal solution at 95 °C for 24 h and annealed at temperature of 440°C

wavelength range and ~25 to 45% in the UV wavelength range [36].

The absorbance spectra of nanomoss Nb_2O_5 (sample A, B, C and D) measured in the wavelength of 200 to 800 nm are presented in Fig. 7. The slope of the absorbance spectra are corresponding to the band gap energy for the nanomoss Nb_2O_5. The band gap value can be calculated directly from the absorbance graph by using the energy-wavelength relationship equation [42];

$$E = hf = hc/\lambda = 1240\ \text{eV nm}/\lambda, \quad (1)$$

where E is energy, h is Plank's constant (6.62606957 × 10–34 J.s), f is frequency, c is light velocity (2.99792458 × 108 m/s) and λ is the incident wavelength value which is determine from the cross link of the edge slope of absorbance spectra, as presented in Fig. 7. It is revealed that the band gap of the sample A, B, C and D of nanomoss Nb_2O_5 are about 3.483, 3.147, 3.792 and 3.123 eV, according to the absorbance edges at about 356, 394, 327 and 397 nm, respectively. The results indicate that the sample B and D has band gap energy lower than excited UV light source, thus this properties make them a suitable candidate for UV sensor application.

Due to low reflectance properties offered by this kind of film structure, they are advantageous for potential use in UV photo detection as well as many other applications. In order to evaluate the nanomoss Nb_2O_5 based UV sensor, time-resolved photoresponse test is performed using 365 nm UV light with an optical power density of 750 μW/cm^2 at a bias voltage of 10 V. Since the crystalline of nanomoss Nb_2O_5 film is obtained after annealing for 60 min at 440 °C, only sample B and D are used to fabricate the UV sensors.

Figure 8 represents the time-resolved photoresponse of the nanomoss Nb_2O_5 based UV sensor. Photoresponses produced by the UV sensors when exposed them under the ON–OFF condition of UV illumination. The plot demonstrates that the photocurrent, I_{ph} of sample B and D is 0.26 and 0.95 μA in magnitude at 10 V when exposed under the 365 nm wavelengths light, respectively. Meanwhile the magnitude of the dark current, I_{dark} for sample B dan D is low as 0.16 and 0.5 μA at 10 V, respectively. As a result, the ratio of photocurrent to the dark current (on/off ratio) which is also defined the sensitivity of the UV sensor for sample B and D is approximately 1.5 and 2,

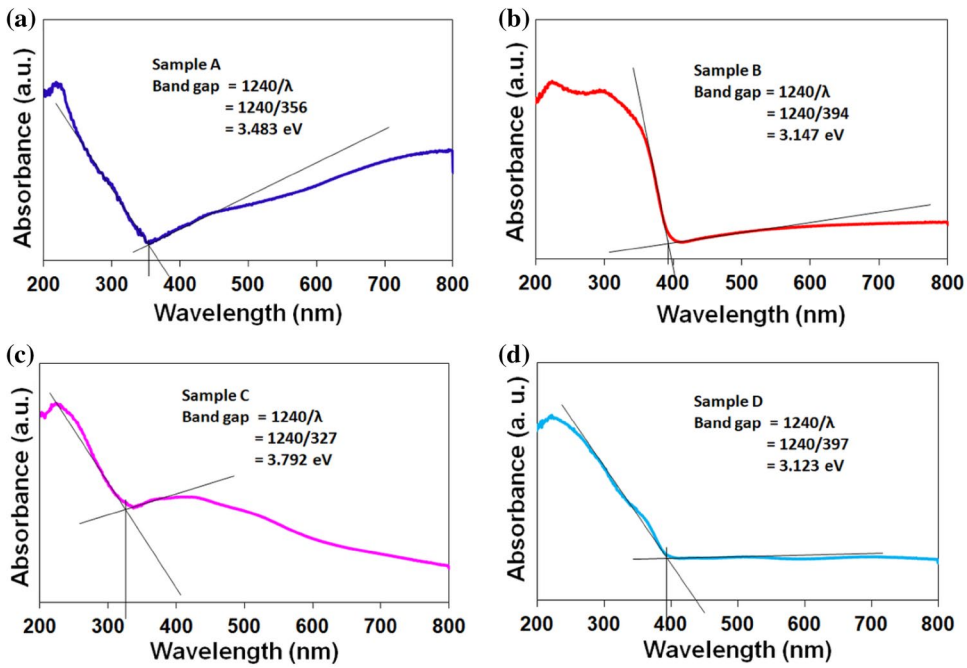

Fig. 7 UV–Vis absorption spectra of nanomoss Nb_2O_5; **a** sample A, **b** sample B, **c** sample C and **d** sample D. The band gap value for each sample was determined by utilize the energy-wavelength relationship; E = hc/λ

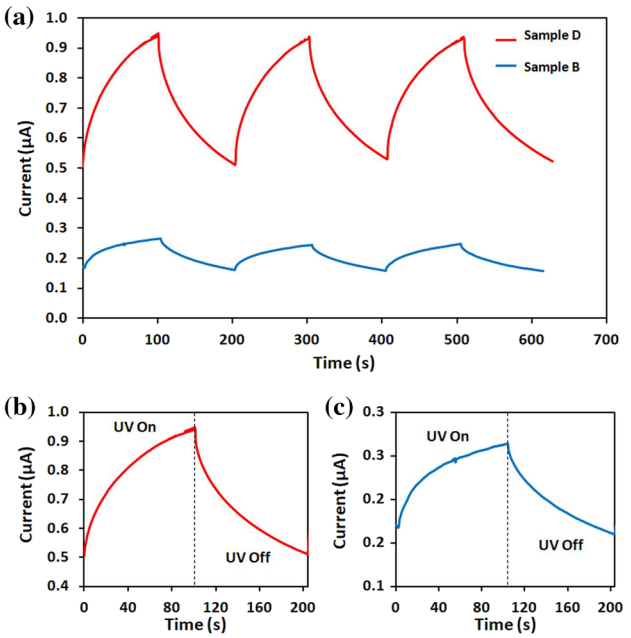

Fig. 8 **a** Photoresponse spectra of the UV sensor using nanomoss Nb_2O_5 films synthesized in 0.5 M (sample B) and 1.65 M (sample D) of NH_4F solution and annealed at 440 °C for 60 min under UV illumination (365 nm, 750 μW/cm^2) and a 10 V bias. Comparison of the response transients of (**b**) sample D and **c** sample B under UV on/off condition

respectively. The results show that the UV sensor based sample D exhibit the highest sensitivity. According to the previous research, the responsivity (R) of nanomoss Nb_2O_5 based UV sensor can be estimated using the following equation [43, 44];

$$R = \frac{I_{ph} - I_{dark}}{PS} \tag{2}$$

where I_{ph} is the photocurrent, I_{dark} is the dark current, P is the optical power of UV light source (750 μW/cm^2), and S is the irradiated area on the UV sensor. From the calculation, the reponsivity values of the UV sensors based sample B and D is 0.67 and 2.43 mA/W, respectively.

The UV sensor properties are further characterized by evaluating their photoresponse time. In this case, the rise time and decay time of the sensors is defined as the time required for the peak photocurrent to increase from 10 to 90% or drop from 90 to 10%. Based on the photoresponse spectra in Fig. 8, the rise (decay) time of the UV sensor based sample B and D are about 51.4 s (76.0 s) and 72.4 s (76.8 s), respectively.

The mechanism of the UV sensor is correlates with the adsorption and desorption activity of oxidizing gas molecules which contribute to the sensor's performance [45, 46]. In the dark condition, oxygen molecules are favorable to adsorb onto the Nb_2O_5 film surfaces by capturing free electrons and producing adsorbed oxygen ions. Those generated adsorbed oxygen ions create a barrier near the surfaces and lowered the current value of the UV sensor. While under exposure to UV light, photogenerated electron–hole pairs are generated on the surface of Nb_2O_5 film. Then, the recombination of photogenerated holes with the adsorbed oxygen ions on the surface occur and produce oxygen molecules and significantly annihilate the barrier near the Nb_2O_5 film surface. This process leaves photogenerated electrons in the conduction band, increase the film conductivity and causes to the increment of photocurrent value. When the UV light is switched off, the oxygen molecules are begins to adsorb again onto the Nb_2O_5 film surface and decrease the film's conductivity as well as the current value of the UV sensor. From the photoresponse results, UV sensor based on sample D showed better performance than that of sample B. This can be attributes to the bigger size of hump structure owing by sample D which contributes less scattering effect upon UV light exposure, thus exhibited lower reflectance spectra. Material with low reflectance properties is very important in producing good photodetection devices since the amount of photo-generated charge carriers is proportional to the absorbed photon flux [44]. Other than that, factor such as balance among charge carriers generation, recombination process as well as ion transportation are also plays a very significant role to the efficiency of the UV sensors [47]. Meanwhile, Fang et. al. also reported the photocurrent of the UV sensor can be improved by improving the crystallinity of the oxide films [29]. They found that the crystallinity of the Nb_2O_5 nanobelts improved significantly after annealing in argon condition instead of air and this situation affected the performance of the UV sensor. The UV sensor based Nb_2O_5 nanobelts anneal in air only exhibited sensitivity of 3.3, while for the Nb_2O_5 nanobelts anneal in argon, sensitivity of 9.4 are obtained. List of current researches on UV photodetection performance using Nb_2O_5 and other common oxide films is summarized in Table 3. Based on the performance showed by the nanomoss Nb_2O_5, it can be concluded that they are a suitable candidate for UV sensor and its responsivity show better or comparable compared to other oxides in UV photodetection application. However, it is observed that, there are distinct differences between UV sensor based nanomoss Nb_2O_5 and single Nb_2O_5 nanobelts as well as single Nb_2O_5 nanoplates. The differences are expected due to the small irradiated area (A) of single Nb_2O_5 nanoplates and nanobelts (in the size of micro and nanometer), which significantly affect the responsivity calculation.

Table 3 Comparison of the UV sensor's parameter for nanomoss Nb_2O_5 based UV sensor and other common oxide nanostructures based UV sensor

Photodetector	UV light (nm)	Applied voltage (V)	Photocurrent (dark current)	Rise (decay) time	Responsivity
Nanomoss Nb_2O_5 (sample D) [this work]	365	10	0.95 μA (0.5 μA)	72.4 (76.8) s	2.43 mA/W
Nanomoss Nb_2O_5 (sample B) [This work]	365	10	0.26 μA (0.16 μA)	51.4 (76.0) s	0.67 mA/W
Nb_2O_5 nanotubes [34]	350	1	100 pA (50 pA)	–	–
Single Nb_2O_5 nanobelts [29]	320	1	100 pA (10.6 pA)	–	15.2 A/W
Single Nb_2O_5 nanoplates [44]	320	1	59.9 pA (< 1 pA)	28 (12.0) s	24.7 A/W
ZnO nanoparticles [45]	325	1	0.03 μA (0.4 pA)	48 (0.9) s	0.1 mA/W
ZnO nanowires FET [48]	365	1	40 μA (15 μA)	0.027 (0.070) s	–
ZnO Nanoflowers/MoS_2 [49]	350	1	–	61 (90.0) s	0.899 mA/W
ZnO nanorods [50]	365	1.8	0.129 mA (61.6 μA)	–	0.199 A/W
Au/double-layer TiO_2 nanostructure [51]	365	1	163.6 μA (2.97 nA)	–	136.4 A/W
TiO_2 nanowires [52]	254	10	47 nA (61.8 pA)	–	–
TiO_2 nanowires [52]	365	10	38 nA (63.3 pA)	–	–
Zinc oxide nanorods / reduced graphene oxide bilayer [53]	365	5	4.3 μA (0.25 μA)	–	180 mA/W

4 Conclusions

In this work, we successfully demonstrate the fabrication of nanomoss Nb_2O_5 films by conducting simple and low cost synthesis method using hydrothermal based etching agent-assisted process. These films were obtained using a temperature lower than 100 °C in DIW solution consisting of 0.5 and 1.65 M of NH_4F and annealed in air at 440 °C for 40 and 60 min. The increase of annealing duration to 60 min has produced hump structure on the nanomoss Nb_2O_5 films and improved their crystallinity, thereby exhibiting low reflectance value around 2.73 to 26.0% at UV wavelength during characterization with UV–Vis Spectrophotometer. The photoresponse measurements at wavelength of 365 nm were conducted on two sample of nanomoss Nb_2O_5 based UV sensors. The UV sensor with a bigger size of hump structure which is synthesized in 1.65 M of NH_4F and annealed for 60 min demonstrated the best performance with sensitivity (ratio of photocurrent to the dark current) of 2.0. The presented work is the first report on nanomoss Nb_2O_5 films as a UV sensor, and further investigations are required to explore their potential applications. Based on the performance showed by the nanomoss Nb_2O_5 based UV sensors, it can be concluded that they are a suitable candidates as other oxides in UV photodetection.

Acknowledgements The authors are grateful to the Fundamental Research Grant Scheme (FRGS) (Project Code: 600-IRMI/FRGS 5/3 (081/2017)), Ministry of Education, Malaysia. Thanks also to Institute of Research Management and Innovation (IRMI), Universiti Teknologi MARA (UiTM) and the Deanship of Scientific Research, King Saud University (KSU) for their support through Vice Deanship of Scientific Research Chairs. The authors would like to express gratitude to Mohd Azlan Jaafar, Nurul Wahida Aziz and Salifairus Mohammad Jafar from NANO-SciTech Centre, Institute of Science, UiTM for their assistance whom plays significant roles in our work.

References

1. L. Fei, X. Dongfeng, Fabrication of Nb_2O_5 nanotrees with controlled branching degrees. Physica Scripta. **2010**, 014074 (2010)
2. H. Wen, Z. Liu, J. Wang, Q. Yang, Y. Li, J. Yu, Facile synthesis of Nb_2O_5 nanorod array films and their electrochemical properties. Appl. Surf. Sci. **257**, 10084 (2011). https://doi.org/10.1016/j.apsusc.2011.07.001
3. H. Luo, M. Wei, K. Wei, Synthesis of Nb_2O_5 nanosheets and its electrochemical measurements. Mater. Chem. Phys. **120**, 6 (2010)
4. R. Abdul Rani, A.S. Zoolfakar, J. Subbiah, J.Z. Ou, K. Kalantar-zadeh, Highly ordered anodized Nb_2O_5 nanochannels for dye-sensitized solar cells. Electrochem. Commun. **40**, 20 (2014). https://doi.org/10.1016/j.elecom.2013.12.011
5. R.A. Rani, A.S. Zoolfakar, J.Z. Ou et al., Reduced impurity-driven defect states in anodized nanoporous Nb_2O_5: the possibility of improving performance of photoanodes. ChemComm. **49**, 6349 (2013). https://doi.org/10.1039/c3cc42998a
6. J.Z. Ou, R.A. Rani, M.H. Ham et al., Elevated temperature anodized Nb_2O_5: a photoanode material with exceptionally large photoconversion efficiencies. ACS Nano **6**, 4045 (2012)
7. C. Nico, T. Monteiro, M.P.F. Graça, Niobium oxides and niobates physical properties: review and prospects. Prog. Mater. Sci. **80**, 1 (2016). https://doi.org/10.1016/j.pmatsci.2016.02.001
8. I. Zhitomirsky, Electrolytic deposition of niobium oxide films. Mater. Lett. **35**, 188 (1998)
9. K. Kamada, M. Mukai, Y. Matsumoto, Anodic dissolution of tantalum and niobium in acetone solvent with halogen additives for electrochemical synthesis of Ta_2O_5 and Nb_2O_5 thin films. Electrochimica Acta. **49**, 321 (2004). https://doi.org/10.1016/j.electacta.2003.08.014
10. T.-Y. Cho, K.-W. Ko, S.-G. Yoon et al., Efficiency enhancement of flexible dye-sensitized solar cell with sol–gel formed Nb_2O_5 blocking layer. Curr. Appl. Phys. **13**, 1391 (2013). https://doi.org/10.1016/j.cap.2013.04.012

11. M.P.F. Graca, A. Meireles, C. Nico, M.A. Valente, Nb_2O_5 nanosize powders prepared by sol-gel—structure, morphology and dielectric properties. J. Alloys Compd. **553**, 177 (2013). https://doi.org/10.1016/j.jallcom.2012.11.128
12. A. Verma, P.K. Singh, Sol-gel derived nanostructured niobium pentoxide thin films for electrochromic applications. Indian J. Chem. Sect. Inorg. Bio-Inorg. Phys. Theor. Anal. Chem. **52**, 593 (2013)
13. E. Çetinörgü-Goldenberg, J.-E. Klemberg-Sapieha, L. Martinu, Effect of postdeposition annealing on the structure, composition, and the mechanical and optical characteristics of niobium and tantalum oxide films. Appl. Opt. **51**, 6498 (2012). https://doi.org/10.1364/AO.51.006498
14. K.N. Chen, C.M. Hsu, J. Liu, Y.C. Liou, C.F. Yang, Investigation of antireflection Nb_2O_5 thin films by the sputtering method under different. Depos. Parameters Micromach. **7**, 151 (2016)
15. ÖD. Coşkun, S. Demirela, The optical and structural properties of amorphous Nb_2O_5 thin films prepared by RF magnetron sputtering. Appl. Surf. Sci. **277**, 35 (2013). https://doi.org/10.1016/j.apsusc.2013.03.116
16. A. Dhar, T.L. Alford (2012) Optimization of Nb_2O_5/Ag/Nb_2O_5 multilayers as transparent composite electrode on flexible substrate with high figure of merit. J. Appl. Phys. https://doi.org/10.1063/1.4767662
17. R. Ghosh, M.K. Brennaman, T. Uher et al., Nanoforest Nb_2O_5 photoanodes for dye-sensitized solar cells by pulsed laser deposition. ACS Appl. Mater. Interfaces **3**, 3929 (2011). https://doi.org/10.1021/am200805x
18. S. Hyunjun, C. Dooho, L. Dongsoo et al., Resistance-switching characteristics of polycrystalline Nb_2O_5 for nonvolatile memory application. IEEE Electron Device Lett. **26**, 292 (2005). https://doi.org/10.1109/LED.2005.846592
19. R.A. Rani, A.S. Zoolfakar, A.P. O'Mullane, M.W. Austin, K. Kalantar-Zadeh, Thin films and nanostructures of niobium pentoxide: fundamental properties, synthesis methods and applications. J. Mater. Chem. A **2**, 15683 (2014). https://doi.org/10.1039/c4ta02561j
20. Ü Özgür, Y.I. Alivov, C. Liu et al., A comprehensive review of ZnO materials and devices. J. Appl. Phys. **98**, 041301 (2005). https://doi.org/10.1063/1.1992666
21. K. Kim, M.-S. Kim, P.-R. Cha, S.H. Kang, J.-H. Kim, Structural modification of self-organized nanoporous niobium oxide via hydrogen treatment. Chem. Mater. **28**, 1453 (2016). https://doi.org/10.1021/acs.chemmater.5b04845
22. J. Zhang, T. Liu, Y. Zhang, W. Zeng, F. Pan, X. Peng, Hydrothermal synthesis and growth mechanisms of different ZnO nanostructures and their gas-sensing properties. J. Mater. Sci. **26**, 1347 (2015). https://doi.org/10.1007/s10854-014-2545-3
23. M.N. Asiah, M.F.A.,M.H. Mamat, Z. Khusaimi, S. Abdullah, M. Rusop, Effect of hydrothermal growth temperature on the morphology and structural properties of synthesized TiO2 nanowires. Adv. Mater. Res. **667**, 442 (2013)
24. S.A. Kamaruddin, K.-Y. Chan, M.Z. Sahdan, M. Rusop, H. Saim, ZnO microstructures and nanostructures prepared by Sol-Gel hydrothermal technique. J. Nanosci. Nanotechnol. **10**, 5618 (2010). https://doi.org/10.1166/jnn.2010.2444
25. N.A. Jayah, H. Yahaya, M.R. Mahmood, T. Terasako, K. Yasui, A.M. Hashim, High electron mobility and low carrier concentration of hydrothermally grown ZnO thin films on seeded a-plane sapphire at low temperature. Nanoscale Res. Lett. **10**, 7 (2015). https://doi.org/10.1186/s11671-014-0715-0
26. K.A. Eswar, J. Rouhi, F.S. Husairi et al., Hydrothermal growth of flower-like ZnO nanostructures on porous silicon substrate. J. Mol. Struct. **1074**, 140 (2014). https://doi.org/10.1016/j.molstruc.2014.05.067
27. J. Rouhi, F.S.H.,K.A. Eswar, S.A.H. Alrokayan, H.A. Khan, M. Rusop, Vertical growth of ZnO nanocone arrays on polycarbonate substrate by voltage-assisted chemical bath deposition. Adv. Mater. Res. **1109**, 495 (2015)
28. J.H. Kang, Y. Myung, J.W. Choi et al., Nb_2O_5 nanowire photoanode sensitized by a composition-tuned CdSxSe1-x shell. J. Mater. Chem. **22**, 8413 (2012)
29. X. Fang, L. Hu, K. Huo et al., New ultraviolet photodetector based on individual Nb_2O_5 nanobelts. Adv. Funct. Mater. **21**, 3907 (2011). https://doi.org/10.1002/adfm.201100743
30. J. He, Y. Hu, Z. Wang et al., Hydrothermal growth and optical properties of Nb_2O_5 nanorod arrays. J. Mater. Chem. C **2**, 8185 (2014). https://doi.org/10.1039/c4tc01581a
31. Y. Jerry, Y. Liu, W. Hao et al., Hydrothermally formed functional niobium oxide doped tungsten nanorods. Nanotechnology **24**, 495501 (2013)
32. R.A. Rani, A.S. Zoolfakar, J.Z. Ou, M.R. Field, M. Austin, K. Kalantar-zadeh, Nanoporous Nb_2O_5 hydrogen gas sensor. Sens. Actuators, B **176**, 149 (2013). https://doi.org/10.1016/j.snb.2012.09.028
33. C.D. Cooper, J.F. Mustard, Effects of very fine particle size on reflectance spectra of smectite and palagonitic soil. Icarus **142**, 557 (1999). https://doi.org/10.1006/icar.1999.6221
34. V. Galstyan, E. Comini, G. Faglia, G. Sberveglieri, Synthesis of self-ordered and well-aligned Nb_2O_5 nanotubes. CrystEngComm **16**, 10273 (2014). https://doi.org/10.1039/c4ce01540a
35. M. Joya, J. Barba Ortega, A. Raba Paez, J. da Silva Filho, P. Cavalcante Freire, Synthesis and characterization of nano-particles of niobium pentoxide with. orthorhombic symmetry. Metals **7**, 142 (2017)
36. J.K. Dash, L. Chen, M.R. Topka et al., A simple growth method for Nb_2O_5 films and their optical properties. RSC Adv. **5**, 36129 (2015). https://doi.org/10.1039/c5ra05074j
37. P. Amaravathy, S. Sowndarya, S. Sathyanarayanan, N. Rajendran, Novel sol gel coating of Nb2O5 on magnesium alloy for biomedical applications. Surf. Coat. Technol. **244**, 131 (2014). https://doi.org/10.1016/j.surfcoat.2014.01.050
38. X. Jin, C. Liu, J. Xu, Q. Wang, D. Chen, Size-controlled synthesis of mesoporous Nb2O5 microspheres for dye sensitized solar cells. RSC Adv. 4, 35546 (2014). https://doi.org/10.1039/c4ra06101b
39. D.C. Castro, R.P. Cavalcante, J. Jorge et al., Synthesis and characterization of mesoporous Nb2O5 and its application for photocatalytic degradation of the herbicide methylviologen. J. Braz. Chem. Soc. **27**, 303 (2016)
40. S. Ge, H. Jia, H. Zhao, Z. Zheng, L. Zhang, First observation of visible light photocatalytic activity of carbon modified Nb_2O_5 nanostructures. J. Mater. Chem. **20**, 3052 (2010). https://doi.org/10.1039/b923586h
41. F. Khan, S.-H. Baek, N. Ahmad et al., Correlation between reflectance and photoluminescent properties of al-rich ZnO nano-structures. Met. Mater. Int. **21**, 561 (2015). https://doi.org/10.1007/s12540-015-4376-z
42. A. Elaziouti, N. Laouedj, A. Bekka, R.-N. Vannier, Preparation and characterization of p–n heterojunction $CuBi_2O_4$/CeO_2 and its photocatalytic activities under UVA light irradiation. JKSUS. **27**, 120 (2015). https://doi.org/10.1016/j.jksus.2014.08.002
43. M.H. Mamat, M.F. Malek, N.N. Hafizah, Z. Khusaimi, M.Z. Musa, M. Rusop, Fabrication of an ultraviolet photoconductive sensor using novel nanostructured, nanohole-enhanced, aligned aluminium-doped zinc oxide nanorod arrays at low immersion times. Sens. Actuators B **195**, 609 (2014). https://doi.org/10.1016/j.snb.2014.01.082
44. H. Liu, N. Gao, M. Liao, X. Fang, Hexagonal-like Nb_2O_5 nanoplates-based photodetectors and photocatalyst with high performances. Sci. Rep. **5**, 7716 (2015). https://doi.org/10.1038/srep07716

45. J.H. Jun, H. Seong, K. Cho, B.-M. Moon, S. Kim, Ultraviolet photodetectors based on ZnO nanoparticles. Ceram. Int. **35**, 2797 (2009). https://doi.org/10.1016/j.ceramint.2009.03.032
46. M.H. Mamat, M.I. Che Khalin, N.N.H. Nik Mohammad et al., Effects of annealing environments on the solution-grown, aligned aluminium-doped zinc oxide nanorod-array-based ultraviolet photoconductive. Sens. J. Nanomater. **2012**, 15 (2012). https://doi.org/10.1155/2012/189279
47. V.D. Mihailetchi, J. Wildeman, P.W.M. Blom, Space-charge limited photocurrent. Phys. Rev. Lett. **94**, 126602 (2005)
48. T.-Y. Tiong, C.-F. Dee, A.A. Hamzah et al., A rapid responding ultraviolet sensor based on multi-parallel aligned ZnO nanowires field effect transistor. Sens. Actuators A **260**, 139 (2017). https://doi.org/10.1016/j.sna.2017.04.022
49. Y.B. Lee, S.K. Kim, Y.R. Lim et al., Dimensional-hybrid structures of 2D materials with ZnO nanostructures via pH-mediated hydrothermal growth for flexible UV photodetectors. ACS Appl. Mater. Interfaces. **9**, 15031 (2017). https://doi.org/10.1021/acsami.7b01330
50. S. Singh, Y. Kumar, H. Kumar et al., A study of hydrothermally grown ZnO nanorod-based metal-semiconductor-metal UV detectors on glass substrates. Nanomater. Nanotechnol. **7**, 1847980417702144 (2017). https://doi.org/10.1177/1847980417702144
51. H. Wang, P. Qin, G. Yi et al., A high-sensitive ultraviolet photodetector composed of double-layered TiO_2 nanostructure and Au nanoparticles film based on Schottky junction. Mater. Chem. Phys. **194**, 42 (2017). https://doi.org/10.1016/j.matchemphys.2017.03.019
52. Y. Wang, J. Cheng, M. Shahid, M. Zhang, W. Pan, A high-performance TiO_2 nanowire UV detector assembled by electrospinning. RSC Adv. **7**, 26220 (2017). https://doi.org/10.1039/c7ra03072j
53. A.A.M. Ali, A.B. Suriani, R.J. Akram, The enhancement Of UV sensor response by zinc oxide nanorods/reduced graphene oxide bilayer nanocomposites film. In: *Journal of Physics: Conference Series*, vol. 1003, 2018, p. 012070